GATA3 controls mitochondrial biogenesis in primary human CD4$^+$ T cells during DNA damage

Lauren A. Callender[1,2,7], Johannes Schroth[1,7], Elizabeth C. Carroll[1,3], Lisa E.L. Romano[4], Eleanor Hendy[5], Audrey Kelly[5], Paul Lavender[5], Arne N. Akbar[6], J. Paul Chapple[1], and Sian M. Henson[1*].

[1]Translational Medicine and Therapeutics, William Harvey Research Institute, Barts and The London School of Medicine and Dentistry, Queen Mary University of London, Charterhouse Square, London EC1M 6BQ, UK

[2]Current address: Clinical Pharmacology and Safety Sciences, R&D, AstraZeneca, Cambridge, UK

[3]Current address: Department of Life Sciences, Institute of Technology Sligo, Sligo, F91 YW50, Ireland

[4]Endocrinology, William Harvey Research Institute, Barts and The London School of Medicine and Dentistry, Queen Mary University of London, Charterhouse Square, London EC1M 6BQ, UK

[5]Peter Gorer Department of Immunobiology and Asthma UK Centre in Allergic Mechanisms of Asthma, King's College London, London SE1 9RT, UK.

[6]Division of Infection and Immunity, Department of Immunology, University College London, London W1T 4JF, UK

[7]Both authors contributed equally

*Correspondence: Dr. Sian M. Henson, s.henson@qmul.ac.uk

Running title: GATA3 regulates mitochondrial biogenesis

Keywords: T cell, CD4, GATA3, metabolism, mitochondria, senescence, DNA damage

Introductory paragraph

GATA binding protein 3 (GATA3) has traditionally been regarded as a lineage-specific transcription factor that drives the differentiation of $CD4^+$ T helper (Th) 2 cells. However, increasing evidence shows that GATA3 is involved in a myriad of processes such as immune regulation, proliferation and maintenance in other T cell and non-T cell lineages. We show here a previously unknown mechanism utilized by $CD4^+$ T cells to increase mitochondrial mass in response to DNA damage through the binding of GATA3, AMP-activated protein kinase (AMPK), peroxisome-proliferator-activated receptor γ co-activator-1α (PGC1α), nuclear factor erythroid 2-related factor 2 (NRF2) and superoxide dismutase 3 (SOD3) to the DNA damage repair (DDR) component ATR. These findings extend the pleotropic nature of GATA3 and highlight the potential for GATA3-targeted cell manipulation for clinical interventions.

Main text

The function of GATA3 in the development of T cells has been well characterised. It is the only member of the GATA family expressed in the T cell lineage[1], and during early T cell development in the thymus GATA3 is essential for $CD4^+$ lineage commitment[2]. Among mature, peripheral $CD4^+$ T cells, GATA3 is also required for Th2 differentiation[3,4]. More recently, GATA3 has been shown to have many functional roles beyond simply controlling $CD4^+$ Th2 cell differentiation. These roles include the development of invariant NKT (iNKT) cells[5], the maturation and homing of natural killer (NK) cells[6] and the regulation and activation of $CD8^+$ T cells[7]. Collectively these studies expand the role of GATA3 in non-T cell and $CD8^+$ T cell lineages, however the role of GATA3 in non-Th2 $CD4^+$ T cells is unknown.

As $CD4^+$ T cells become more highly differentiated they develop a Th1-like phenotype, characterised by increased IFN-γ and decreased IL-4, IL-5 and IL-13 cytokine production[8,9]. Here, we examined the

expression of GATA3 in primary human $CD4^+$ T cell subsets defined by CD45RA and CD27 expression (Extended data figure 1a) – Naive ($CD45RA^+CD27^+$), central memory (CM; $CD45RA^-CD27^+$), effector memory (EM; $CD45RA^-CD27^-$) and effector memory that re-express CD45RA (EMRA; $CD45RA^+CD27^-$)[10,11]. $CD4^+$ EMRA T cells are a highly differentiated population that exhibit many characteristics of cellular senescence such as DNA damage[12], and have Th1-like phenotype[8,9]. Despite this, unstimulated $CD4^+$ EMRA T cells expressed the highest levels of GATA3 when compared to the other three subsets by flow cytometry and qPCR (Figure 1a and extended data figure 1b). Furthermore, the expression of GATA3 remained high in the $CD4^+$ EMRA subset following stimulation (Extended data figure 1c). This observation led us to hypothesize that GATA3 has an alternate function in the $CD4^+$ EMRA subset. In the $CD8^+$ lineage, GATA3 expression was low and remained unchanged amongst the four subsets (Extended data figure 1d).

Cellular metabolism is a crucial regulator of T cell function and fate, and the physiological importance of mitochondria in regard to cell metabolism has been widely appreciated for many years. We have previously shown mitochondrial mass to be lower in $CD8^+$ EMRAs compared to other memory subsets and the mitochondria present to be dysfunctional[13]. Therefore, we sought to investigate the mitochondrial properties of $CD4^+$ T cells subsets. First, we assessed the total mitochondrial mass of $CD4^+$ T cell subsets using the mitochondrial probe; Mitotracker Green. These data revealed that mitochondrial mass increased with differentiation in unstimulated and stimulated $CD4^+$ T cells, with $CD4^+$ EMRA T cells displaying the highest mitochondrial content in both cases (Figure 1b, extended data figure 1e). This observation was further supported by scanning electron microscopy data, which confirmed that $CD4^+$ EMRA T cells had a significantly higher volume of mitochondria (Figure 1c and d). Together with increased mitochondrial mass we also observed increased levels of the co-transcriptional regulator important for mitochondrial biogenesis; PGC1α, in $CD4^+$ EMRA T cells by flow cytometry and qPCR (Figure 1e, extended data figure 1f). Collectively

these data positively correlated with the GATA3 expression data and suggested a possible link between GATA3 and mitochondrial biogenesis.

To determine whether the increased mitochondrial mass was of functional importance we used tetramethylrhodamine (TMRE) to measure mitochondrial membrane potential (ΔΨm) in $CD4^+$ T cell subsets. Notably, we observed that a greater proportion of $CD4^+$ EMRA T cells had hyperpolarised mitochondria compared with the other three subsets (Figure 2a). Hyperpolarised mitochondria have been shown to be a source of reactive oxygen species (ROS) in both macrophages[14] and $CD8^+$ tumour infiltrating lymphocytes[15]. Therefore, we examined intracellular ROS and found that $CD4^+$ EMRA T cells also displayed high levels of ROS (Figure 2b). However, although the levels of ROS were significantly higher in the $CD4^+$ EMRA T cells compared with all other subsets, the ROS/mitochondria ratio was unchanged (Figure 2b). This led us to postulate that increased mitochondrial mass in $CD4^+$ EMRA T cells is a protective mechanism to ensure that $CD4^+$ EMRA T cells are able to adequately buffer the excess ROS and prevent further DNA damage.

We next investigated whether increased mitochondrial mass and hyperpolarised mitochondrial membrane potential in $CD4^+$ EMRA T cells led to metabolic reprogramming. To do this we used a mitochondrial stress test to measure the bioenergetics profiles of TCR stimulated CD45RA/CD27 defined $CD4^+$ T cell subsets (Figure 2c). The mitochondrial stress test includes the addition of four pharmacological drugs that manipulate oxidative phosphorylation (OXPHOS), which were added in succession to alter the bioenergetics profiles of the mitochondria. Upon stimulation, naïve $CD4^+$ T cells had a significantly lower basal oxygen consumption rate (OCR) compared to the memory T cells, however no differences were found amongst the three memory subsets (Figure 2d). The extracellular acidification rate (ECAR), a marker of lactic acid production and glycolysis, was highest in the EM and EMRA $CD4^+$ subsets compared to naïve and CM subsets (Figure 2e). Furthermore, the

spare respiratory capacity (SRC), a measure of how well mitochondria are potentially able to produce energy under conditions of stress, was also significantly lower in the naïve $CD4^+$ T cells but unchanged in the three memory subsets (Figure 2f). $CD4^+$ T cells remained metabolically quiescent with no stimulation (Extended data figure 1g). Collectively, these data suggest that despite having hyperpolarised mitochondria $CD4^+$ EMRA T cells are able to maintain normal T cell metabolism.

DNA damage can severely affect the function of DNA and plays a major role in age-related diseases and cancer[16]. DNA damage can occur for a number of reasons. For instance, cells which undergo rapid proliferation tend to accumulate DNA damage, as well as many end-stage cells that have undergone replicative senescence in response to telomere dysfunction[17–19]. In support of this we found that DNA damage, determined by an increase in the histone marker for double stranded DNA breaks; yH2AX, was significantly higher in the $CD4^+$ EMRA T cells when compared with the other three subsets (Figure 3a). To further verify this, activation of the downstream regulator of the DNA damage response; p53 was determined by the phospho-p53/p53 ratio. Indeed, we found that activated p53 increased with differentiation, with the naive $CD4^+$ T cells expressing the least and the $CD4^+$ EMRA subset expressing the most (Figure 3a). In addition, $CD4^+$ EMRA T cells appear to accumulate DNA damage in response to ROS faster than the other memory subsets (Figure 3b).

A possible connection between GATA3 and mitochondria has been previously reported. A yeast two-hybrid screen showed that GATA3 is able to interact with the DDR proteins; ataxia telangiectasia mutated (ATM) and ataxia telangiectasia and Rad3-related (ATR) as well as PGC1α[20]. Immunoprecipitation (IP) assays showed that GATA3 and PGC1α were bound to the ATR in $CD4^+$ T cells (Figure 3c). Furthermore, $CD4^+$ EMRA T cells had the highest levels of GATA3 and PGC1α bound to the ATR in all three repeats (Extended data figure 2a). We next sort to identify other mitochondrial regulators that may also be upregulated by GATA3 using chromatin immunocleavage.

These data revealed that in resting naïve T cells, GATA3 may be recruited directly or indirectly to the promoter regions of a number of genes including NRF1, NRF2, SOD3, as well as PGC1α (Figure 3d). To mimic DNA damage, we incubated $CD4^+$ T cells with hydroxyurea; a DNA replication inhibitor known to induce DNA double strand breaks primarily via the ATR-Chk1 pathway[21,22]. Overnight incubation with hydroxyurea resulted in a significant increase in Tom20, a major outer mitochondrial membrane receptor and therefore mitochondrial marker, and GATA3 using confocal analysis. The increased expression of GATA3 was located in both the cytoplasm and nucleus (Figure 3e, Extended data figure 2b). In addition, flow cytometry revealed a significant increase in phospho-p53, intracellular PGC1α and an increased mitochondrial content, determined by elevated Mitotracker green staining (Extended data figure 2c-e). Furthermore, IP assays showed that treatment with hydroxyurea increased the amount of PGC1α, NRF2 and SOD3 bound to GATA3 (Figure 3f, Extended data figure 2f). Interestingly we found no interaction between NRF1 and GATA3, suggesting that GATA3 may regulate NRF1 at the level of transcription rather than via protein-protein interactions (data not shown).

In order to determine the requirement for ATR activation in regulating mitochondrial biogenesis we used the ATR inhibitor AZD6738 (Ceralasertib). We found that inhibition of the ATR following hydroxyurea treatment prevented the increase in mitochondrial biogenesis, bringing mitochondrial mass down to the level observed with stimulation alone (Figure 3g). We then sought to determine the confirmation of the complex through siRNA knockdown of GATA3 followed by pull down of PGC1α. We found ATR present in both the control and GATA3 siRNA lanes (data not shown) suggesting that while ATR activity is required for complex formation its assembly may not be sequential.

To verify that GATA3 can directly regulate mitochondrial biogenesis and fitness we used small

interfering RNA (siRNA) to reduce GATA3 expression in purified human $CD4^+$ T cells following activation (Extended data figure 3a-c). Transfection with GATA3 siRNA led to a significant decrease in both the levels of PGC1α and Mitotracker Green staining (Figure 4a, b; Extended data figure 3d), signifying a marked reduction in mitochondrial mass. Confocal microscopy examination of Tom20 (Figure 4c) showed a significant reduction in both mitochondrial mass (Extended data figure 3e) and volume (Extended data figure 3f) in Jurkat cells following transfection with GATA3 siRNA. TMRE staining revealed a dramatic shift from hyperpolarised to hypopolarised mitochondrial membrane potential in the GATA3 siRNA transfected $CD4^+$ T cells but not the scrambled siRNA transfected $CD4^+$ T cells (Figure 4d). Moreover, transfection with GATA3 siRNA dramatically inhibited the ability of $CD4^+$ T cells to perform OXPHOS when compared with $CD4^+$ T cells transfected with negative control scrambled siRNA (Figure 4e). Basal OCR and SRC were significantly decreased in the GATA3 siRNA transfected $CD4^+$ T cells (Figure 4f). $CD8^+$ T cells transfected with GATA3 siRNA showed no difference in their bioenergetic profiles when compared with negative control scrambled siRNA (Extended data figure 3g). Furthermore, we failed to observe a switch to glycolysis with GATA3 knockdown, as ECAR did not significantly increase with the addition of oligomycin (Figure 4g). Additionally, chromatin immunocleavage demonstrated that GATA3 also bound to the promoter regions of hexokinase 1 and 2, together with SLC2A1 suggesting that GATA3 knockdown could interfere with glycolytic metabolism (Extended data figure 4a). A finding that is supported by data showing that GATA3 controls glycolysis through the negative regulation of PPARγ[23].

We then sought to determine how GATA3 regulates the activity of PGC1α. We found that AMPK was highly expressed in the $CD4^+$ EMRA subset ex-vivo (Figure 4h, Extended data figure 4b) and expression remained high following stimulation (Extended data figure 4c, d), which correlated to the level of γH2AX observed in $CD4^+$ EMRA T cells (Figure 3a). Indeed it has been reported that the ATM plays a role in mitochondrial biogenesis through AMPK activation in response to DNA

damage[24]. Furthermore, chromatin immunocleavage revealed that GATA3 can be recruited to the promoter regions of both AMPK1 and 2 (Figure 4i). While c-myc has been shown to play a role in B cell mitochondrial biogenesis[25], we find no evidence for its involvement in this model. Despite chromatin immuocleavage showing GATA3's recruitment to the promoter region of c-myc (Extended data figure 4e) we do not see any change in c-myc expression post-transcriptionally following knockdown of GATA3 (Extended data Figure 4f). Mitochondrial biogenesis mediated via c-myc is thought to be regulated by NRF1 gene targets[26], as we failed to find evidence of NRF1 involvement we believe that NRF1-c-myc do not control mitochondrial biogenesis through DNA damage. Instead, we postulate a feed-forward loop involving GATA3 and AMPK, whereby AMPK phosphorylates PGC1α (Figure 4j).

Finally, we sought to investigate the functional consequence of preventing increased mitochondrial mass in response to DNA damage. We prevented mitochondrial biogenesis using doxycycline, an antibiotic that inhibits mitochondrial protein translation[27]. When doxycycline was given following hydroxyurea treatment, we observed a reduction in mitochondrial content as well as a dramatic increase in ROS production (Figure 4k; extended data figure 4g). Moreover, the decline in mitochondrial content led to a rise in apoptosis, evident by the sharp increase in annexin expression (Figure 4l; extended data figure 4h). Taken together, these data provide evidence that GATA3 modulates mitochondrial biogenesis, cell metabolism, as well as antioxidant response regulating proteins via a nucleus to mitochondria signalling axis to maintain the viability of these cells during DNA damage.

Mechanistically, GATA3 interacts with the DDR protein ATR, activating the PGC1a signalling pathway to promote mitochondrial biogenesis in $CD4^+$ T cells, and interacts with antioxidant proteins NRF2 and SOD3, which are important for protecting cells against oxidative damage[28,29]. Importantly, as

DDR mechanisms are widely conserved mechanisms, it is likely for this mechanism to not be restricted to the lymphocyte lineage alone. GATA3 is expressed in various cell types outside the haematopoietic system and has been implicated in the tumorigenesis of many cancers, such as luminal breast cancer[30], neuroblastoma[31] and endometrial carcinomas[32].

GATA3-positive breast cancers have been shown to be highly differentiated, with resulting tumours two-fold larger in size than control tumours. In contrast, GATA3-negative breast cancers form poorly differentiated tumours and are highly metastatic[33]. However, despite being associated with low metastatic potential and therefore a more favourable prognosis, GATA3-positive tumours are also associated with resistance to chemotherapy[34]. In light of the present study, we hypothesize that the accumulation of DNA damage generated during chemotherapy recruits GATA3, allowing GATA3-positive tumours to maintain mitochondrial fitness and evade chemotherapy induced apoptosis. However, additional examination of GATA3 and its contribution to mitochondrial biogenesis in cancer is needed to confirm this.

More broadly, our results implicate that transcription factors are likely to serve additional functions after their initial roles in differentiation. This is already the case for the Th1 differentiation marker; T-bet, which is also known to be crucial for long-term memory in $CD8^+$ T cells[35,36] and maturation of NK cells[37]. More recently; STAT5, which has traditionally been associated with cytokine signalling and JAK kinases[38], has now also been identified as a central regulator of naïve $CD4^+$ T cell metabolism[39]. Furthermore, although the GATA proteins have restricted expression patterns to some extent their functions can be interchangeable. For example, GATA1, - 2, and-4 can all activate the expression of GATA3 target genes IL-4 and IL-5 and repress IFNγ in T cells[40]. Interestingly, GATA4 has previously been shown to become activated in the presence of the ATM and ATR, resulting in the induction of senescence and a senescence associated secretory phenotype (SASP) in human

fibroblasts[41]. These functional overlaps suggest that other GATA proteins may also be capable of influencing cell metabolism.

In summary, our data identifies a previously unknown role for GATA3 in response to DNA damage, revealing it as a key mediator of mitochondria biogenesis and cell metabolism. Our findings extend the pleotropic nature of GATA3, demonstrating that more focus should be placed on investigating the role of other transcription factors in later stages of cell development to assess their full range of their abilities. Furthermore, the widespread expression of GATA3 in numerous cancers demonstrate the potential for GATA3-targeted manipulation for clinical interventions.

Experimental procedures

Blood sample collection and isolation

Ethics for blood collection were approved by the NRES Committee North East (REC reference: 16/NE/0073) and all subjects provided written informed consent. Heparinized peripheral blood samples were taken from healthy volunteers, average age 41 years ± 5. Healthy volunteers were individuals who had not had an infection or immunisation within the last month, no known immunodeficiency, and had not received any other immunosuppressive medications within the last 6 months. Peripheral blood mononuclear cells (PBMCs) were isolated using Ficoll-Paque (Amersham Biosciences).

Flow cytometric analysis and cell sorting

Flow cytometric analysis was performed on approximately 1 x 10^6 PBMCs per sample. Cells were incubated in the dark with the Zombie_NIR live/dead stain (Biolegend) and the following antibodies: CD4 PE-CF594 (RPA-T4) from BD Biosciences, CD45RA BV605 (HI100) and CD27 BV421 (O323) from BioLegend, for 15 minutes at room temperature. For intracellular staining, the following antibodies were used: GATA3 AF488 (16E10A23) and γH2AX AF488 (2F3) from BioLegend, PGC1α (3G6), pAMPK (Thr172, 40H9), p53 Alexa Fluor 647 (1C12) and p-p53 Alexa Fluor 647 (Ser15, 16G8) from Cell Signalling Technology, c-myc (9E10) from Santa Cruz Biotechnology and goat anti-rabbit IgG H&L Alexa Fluor 488 from Abcam.

Detection of GATA3, PGC1α, p53, γH2AX and p-p53 were carried out directly ex vivo. The Foxp3 Transcription Factor Staining Buffer Kit (Biolegend) was used for staining GATA3, p53, γH2AX and p-p53. Following surface staining PBMCs were incubated with the FOXP3 Fix/Perm buffer for 20 minutes in the dark at room temperature followed by incubation with the FOXP3 Perm buffer (10X) for 15 minutes in the dark at room temperature. Finally cells were incubated with the FOXP3 Perm

buffer (10X) and appropriate amount of the antibody being used for 30 minutes in the dark and room temperature. The FIX & PERM® Cell Permeablilisation Kit (Life Technologies) was used to enable intracellular staining of PGC1α. Immediately after surface staining, PBMCs were fixed with Reagent A for 15 minutes in the dark at room temperature. Next the cells were permeabilised with Reagent B plus 10% goat serum and recommended volume of primary intracellular antibody. Cells were incubated for 20 minutes in the dark at room temperature followed by a 20 minute incubation with the secondary antibody.

All samples were acquired on a LSR Fortessa (BD Biosciences) equipped with four lasers: 488 nm blue laser, 561 nm yellow green laser, 641 red laser and 405 nm violet laser and data was analysed using FlowJo software.

$CD4^+$ T cells were purified using anti-CD4+ conjugated microbeads (Miltenyi Biotec) according to the manufacturer's instructions. Positively selected CD4+ T cells were labelled with CD27 FITC (O323) and CD45RA APC (HI100) (both from BD Biosciences) and sorted using a FACSAria (BD Biosciences). The purity of CD4 T-cell subsets were assessed by flow cytometry.

Mitochondrial measurements

For mitochondrial mass, PBMCs were incubated with 100 nM MitoTracker Green FM (Invitrogen™) for 30 minutes at 37°C, 5% CO2. ROS was measured using Dihydroethidium (DHE; ThermoFisher), 5µM MitoSOX was incubated with labelled PBMCs for 20 minutes at 37oC, 5% CO2. Mitochondrial membrane potential (MMP) was investigated using Tetramethylrhodamine (TMRE; ThermoFisher Scientific) 2 µM TMRE was incubated with PBMCs for 30 minutes at 37°C, 5% CO2. Following mitochondrial staining, samples were surface stained and then left unfixed and immediately analysed on an LSR Fortessa (BD Biosciences).

To assess mitochondrial morphology by confocal microscopy, Jurkat cells were plated onto microscope slides then fixed and permed using the FIX & PERM® Cell Permeablilisation Kit (Life Technologies) to enable intracellular labelling. Cells were incubated with Reagent A (Fixation Medium) for 15 minutes at room temperature, then Reagent B (Permeablisaton Medium) plus 10% goat serum and Tom20 (F-10, Santa Cruz) for 20 minutes at room temperature followed incubation with the secondary antibody. Finally, cells were incubated with 4',6-diamidino-2-phenylindole (DAPI) (ThermoFisher Scientific) for 10 minutes at room temperature in the dark, and then fixed in 2% paraformaldehyde. Samples were imaged on a Zeiss LSM 880 confocal microscope with a X 63 oil-immersion objective lens. Excitation was at 488 nm from an argon-ion laser. Fluorescence detection was in the green; 500 – 570 nm and UV; 405 nm channel. Quantification of image data was performed by measuring the intensity of the 500 – 570 nm channel using ZEN-imaging. Imaris Image Analysis software was used to determine mitochondrial volume through surface 3D rendering of Z-stack images.

Transmission electron microscopy studies

CD27/CD45RA defined $CD4^+$ T cell subsets were isolated and fixed in 2% paraformaldehyde, 1.5% glutaraldehyde in 0.1 m phosphate buffer pH 7.3. They were then osmicated in 1% OsO4 in 0.1M phosphate buffer, dehydrated in a graded ethanol-water series, cleared in propylene oxide and infiltrated with Araldite resin. Ultra-thin sections were cut using a diamond knife, collected on 300 mesh grids, and stained with uranyl acetate and lead citrate. The cells were viewed in a Jeol 1010 transmission electron microscope (Jeol) and imaged using a Gatan Orius CCD camera (Gatan). Mitochondrial volume density (percentage of T cell volume occupied by mitochondria) was determined from EM images using a point-counting method using image J.

Live cell metabolic assays

The Cell Mito Stress Test was performed on a Seahorse XFe96 Analyser (Agilent) to assess mitochondrial function and OXPHOS. Seahorse sensor cartridges were incubated at 37°C in a non-CO2 incubator overnight with Seahorse XF Calibrant pH 7.4 (Agilent) to rehydrate the sensor probes. The assay was performed in RPMI-1640 buffer without phenol red and carbonate buffer (Sigma-Aldrich) containing 25 mM glucose, 2 mM L-glutamine and 1 mM pyruvate with a pH of 7.4. The stress test was performed using 1 µM Oligomycin, 1.5 µM flurocarbonyl cyanide phenylydrazone (FCCP), 100 nM rotenone, and 1 µM antimycin A (Agilent). Cells were stimulated with 1 µg/µL of anti-CD3 and 5 ng/mL IL-2 15 minutes prior to each metabolic test. Metabolic measurements were calculated according to the manufacturer's guidelines.

Immunoprecipitation

For immunoprecipitation experiments the Chk1 or GATA3 antibody was incubated with Red Protein G Affinity beads (Sigma-Aldrich) for 1 hour at 4°C on a shaker to allow the antibody to bind to the beads. Cell lysates were collected in RIPA buffer plus inhibitors (protease: complete mini Roche; 11836153001, and phosphatases: cocktail set II Calbiochem; 524625) and then incubated with the antibody-bead mix overnight at 4°C on a shaker. The following morning, samples were centrifuged, and the supernatant was discarded leaving only the proteins able to bind to Chk1. SDS-polyacrylamide electrophoresis and western blotting of GATA3 and PGC1α was then carried performed as described above. The protein was detected via chemiluminescence, by means of the ECL system (GE Healthcare).

Hydrogen peroxide experiments

Oxidative stress was induced by the addition of 200 µM H_2O_2 for 1 hour. After this time the

expression of γH2AX in CD27/CD45RA defined $CD4^+$ T cell subsets was assessed by flow cytometry.

Hydroxyurea experiments

To induce DNA damage, PBMCs were incubated with 400 µM hydroxyurea for 48 hours. Following DNA damage, an immunoprecipitation using the Chk1 antibody was carried out to assess GATA3 and PGC1α binding, apoptosis and mitochondrial properties were examined via flow cytometry. Where indicated 1µM AZD6738 or 50 µM doxycycline was also added to the cell cultures, DMSO was added to control samples.

Apoptosis experiments

PBMCs were incubated with the desired inhibitors described above, after which time the cells were stained using the Annexin V apoptosis kit (Biolegend) according to the manufacturer's instructions.

qPCR of GATA3 and PGC1α

RNA from CD27/CD45RA defined $CD4^+$ T cell subsets was isolated using the RNeasy kit (Qiagen) according the manufactures instructions. Transcripts were quantified using the AccuScript high fidelity RT-PCR system (Agilent) according the manufactures instructions. Primer sequences were as follows: GATA3F: GCC CCT CAT TAA GCC CAA G; GATA3R: TTG TGG TCT GAC AGT TCG; PGC1α F: TCT GAG TCT GTA TGG AGT GAC AT; PGC1a R: CCA AGT CGT TCA CAT CTA GTT CA.

GATA3 siRNA knockdown experiments

GATA-3 and scrambled siRNA (GATA3; 5'-/5Alex647N/UAG GCG AAU CAU UUG UUC AAA-3', Scrambled; 5' CCU GUU CUU AAA AUA GUA GGC 3') were dissolved to a final concentration of 10 µM in electroporation buffer, transferred to an electroporation cuvette and electroporated using program T-023 on an Amaxa Nucleofector (Lonza Bioscience). Cell were then left to recover for 24

to 48 hours in fresh RPMI-1640 media. Primary human CD4+ T cells were stimulated with 1 µg/µL of anti-CD3 and 5 ng/mL IL-2 for 24 hours prior to transfection whereas Jurkat cells were left unstimulated.

Chromatin immunocleavage.

Chromatin Immunocleavage was undertaken using proteinA-micrococcal nuclease (pA-MN)[42] repurposed to Cut and Run[43]. Naïve primary human T cells were isolated as previously described[44]. Following nuclear isolation, regions of chromatin bound by GATA3 were identified using a mouse anti-GATA3 antibody (HG3-31) Santa Cruz Biotechnology followed by pA-MN. DNA was isolated from eluted chromatin, libraries were prepared using NEBNext® Ultra II DNA Library Prep Master Mix Set and Multiplex Oligos for Illumina® (New England Biolabs). Library quality was assessed using Bioanalyzer 2100 High Sensitivity DNA Gels (Agilent). Libraries were subjected to 50bp single end read sequencing on an HighSeq 2500 (Illumina) in rapid run format and reads were aligned to Human genome hg19 using Bowtie2 (Galaxy v2.2.6)[45] and visualized within the UCSC genome browser.

Statistical analysis

GraphPad Prism was used to perform statistical analysis. Statistical significance was evaluated using the paired Student t-test or a repeated-measures ANOVA with the Tukey correction used for post-hoc testing. Differences were considered significant when P was <0.05.

Acknowledgements

This work was supported by the British Heart Foundation (LAC), a Springboard award from the Academy of Medical Science and the Wellcome trust (ECC, SMH), the Rosetrees Trust (SMH). ANA was funded by the Medical Research Council (MR/P00184X/1). The LSM880 confocal used in these studies was purchased through a Barts and the London Charity grant MGU0293. We would also like to thank the CRUK Flow Cytometry Core Service at Barts Cancer Institute (Core Award C16420/A18066) and the BRC Genomics Platform at National Institute of Health Research (NIHR) Biomedical Research Centre at Guy's and St. Thomas' Hospitals, London.

Conflict of Interest

The authors have no conflicting financial interests.

Data availability

The data that support the findings of this study are available form the corresponding author upon reasonable request.

Author contributions

LAC, JS and SMH wrote the manuscript, performed the experiments and analysed the data; ECC, EH, AK and PL performed experiments; LELR and JPC assisted with the Tom20 experiments and reviewed the manuscript and ANA reviewed the manuscript.

References

1. Ho, I. C. *et al.* Human GATA-3: a lineage-restricted transcription factor that regulates the expression of the T cell receptor alpha gene. *EMBO J.* **10**, 1187–92 (2018).
2. Hernández-Hoyos, G., Anderson, M. K., Wang, C., Rothenberg, E. V. & Alberola-Ila, J. GATA-3 expression is controlled by TCR signals and regulates CD4/CD8 differentiation. *Immunity* **19**, 83–94 (2003).
3. Zheng, W. P. & Flavell, R. A. The transcription factor GATA-3 is necessary and sufficient for Th2 cytokine gene expression in CD4 T cells. *Cell* **89**, 587–96 (1997).
4. Pai, S.-Y., Truitt, M. L. & Ho, I.-C. GATA-3 deficiency abrogates the development and maintenance of T helper type 2 cells. *Proc. Natl. Acad. Sci.* **101**, 1993–8 (2004).
5. Kim, P. J. *et al.* GATA-3 regulates the development and function of invariant NKT cells. *J. Immunol. (Baltimore, Md 1950)* **177**, 6650–9 (2006).
6. Samson, S. I. *et al.* GATA-3 promotes maturation, IFN-γ production, and liver-specific homing of NK cells. *Immunity* **19**, 701–11 (2003).
7. Tai, T.-S., Pai, S.-Y. & Ho, I.-C. GATA-3 Regulates the Homeostasis and Activation of CD8+ T Cells. *J. Immunol.* **190**, 428–37 (2012).
8. Das, A. *et al.* Effector/memory CD4 T cells making either Th1 or Th2 cytokines commonly co-express T-bet and GATA-3. *PLoS One* **12**, e0186932 (2017).
9. Sakata-Kaneko, S., Wakatsuki, Y., Matsunaga, Y., Usui, T. & Kita, T. Altered Th1/Th2 commitment in human CD4+ T cells with ageing. *Clin. Exp. Immunol.* **120**, 267–73 (2000).
10. Koch, S. *et al.* Multiparameter flow cytometric analysis of CD4 and CD8 T cell subsets in young and old people. *Immun. Ageing* **5**, 6 (2008).
11. Henson, S. M., Riddell, N. E. & Akbar, A. N. Properties of end-stage human T cells

defined by CD45RA re-expression. *Curr. Opin. Immunol.* **24**, 476–81 (2012).

12. Di Mitri, D. *et al.* Reversible Senescence in Human CD4+CD45RA+CD27- Memory T Cells. *J. Immunol.* **187**, 2093–100 (2011).

13. Henson, S. M. *et al.* P38 signaling inhibits mTORC1-independent autophagy in senescent human CD8+ T cells. *J. Clin. Invest.* **124**, 4004–16 (2014).

14. Mills, E. L. *et al.* Repurposing mitochondria from ATP production to ROS generation drives a pro-inflammatory phenotype in macrophages that depends on succinate oxidation by complex II. *Cell* **167**, 457–470 (2016).

15. Siska, P. J. *et al.* Mitochondrial dysregulation and glycolytic insufficiency functionally impair CD8 T cells infiltrating human renal cell carcinoma. *JCI Insight* **2**, 93411 (2017).

16. Hoeijmakers, J. H. J. DNA Damage, Aging, and Cancer. *N. Engl. J. Med.* **361**, 1475–1485 (2009).

17. Hayflick, L. & Moorhead, P. S. The serial cultivation of human diploid cell strains. *Exp. Cell Res.* **25**, 585–621 (1961).

18. Harley, C. B., Futcher, A. B. & Greider, C. W. Telomeres shorten during ageing of human fibroblasts. *Nature* **345**, 458–60 (1990).

19. Richter, T. & Zglinicki, T. von. A continuous correlation between oxidative stress and telomere shortening in fibroblasts. *Exp. Gerontol.* **42**, 1039–42 (2007).

20. Kim, M. A. *et al.* Identification of novel substrates for human checkpoint kinase Chk1 and Chk2 through genome-wide screening using a consensus Chk phosphorylation motif. *Exp. Mol. Med.* **39**, 205–12 (2007).

21. Bianchi, V., Pontis, E. & Reichard, P. Changes of deoxyribonucleoside triphosphate pools induced by hydroxyurea and their relation to DNA synthesis. *J. Biol. Chem.* **261**, 16037–16042 (1986).

22. Timson, J. Hydroxyurea. *Mutat. Res.* **32**, 115–132 (1975).

23. Lee, J. E. & Ge, K. Transcriptional and epigenetic regulation of PPARγ expression during adipogenesis. *Cell Biosci* **4**, 29 (2014).

24. Fu, X., Wan, S., Lyu, Y. L., Liu, L. F. & Qi, H. Etoposide induces ATM-dependent mitochondrial biogenesis through AMPK activation. PLoS One 3, e2009 (2008).

25. Li, F. et al. Myc Stimulates Nuclearly Encoded Mitochondrial Genes and Mitochondrial Biogenesis Graduate Programs in Human Genetics and Molecular Biology. Mol. Cell. Biol. 25, 6225–6234 (2005).

26. Kim, J., Lee, J. H. & Iyer, V. R. Global identification of Myc target genes reveals its direct role in mitochondrial biogenesis and its E-box usage in vivo. PLoS One 3, e1798 (2008).

27. Lamb, R. *et al.* Antibiotics that target mitochondria effectively eradicate cancer stem cells, across multiple tumor types: Treating cancer like an infectious disease. *Oncotarget* **6**, 4569-84 (2015).

28. Nguyen, T., Nioi, P. & Pickett, C. B. The Nrf2-antioxidant response element signaling pathway and its activation by oxidative stress. *J. Biol. Chem* **284**, 13291-5 (2009).

29. Singh, B. & Bhat, H. K. Superoxide dismutase 3 is induced by antioxidants, inhibits oxidative DNA damage and is associated with inhibition of estrogen-induced breast cancer. *Carcinogenesis* **33**, 2601-10 (2012).

30. Mehra, R. *et al.* Identification of GATA3 as a breast cancer prognostic marker by global gene expression meta-analysis. *Cancer Res.* **65**, 11259–11264 (2005).

31. Peng, H. *et al.* Essential role of GATA3 in regulation of differentiation and cell proliferation in SK-N-SH neuroblastoma cells. *Mol. Med. Rep.* **11**, 881–886 (2015).

32. Engelsen, I. B., Stefansson, I. M., Akslen, L. A. & Salvesen, H. B. GATA3 expression in estrogen receptor α-negative endometrial carcinomas identifies aggressive tumors with high proliferation and poor patient survival. *Am. J. Obstet. Gynecol.* **199**, 543.e1–7 (2008).

33. Kouros-Mehr, H. *et al.* GATA-3 Links Tumor Differentiation and Dissemination in a Luminal Breast Cancer Model. *Cancer Cell* **13**, 141–52 (2008).

34. Tominaga, N. *et al.* Clinicopathological analysis of GATA3-positive breast cancers with special reference to response to neoadjuvant chemotherapy. *Ann. Oncol.* **23**, 3051–7 (2012).

35. Juedes, A., Glimcher, L. H., Szabo, S. J., von Herrath, M. & Sullivan, B. M. Antigen-driven effector CD8 T cell function regulated by T-bet. *Proc. Natl. Acad. Sci.* **100**, 15818–23 (2003).

36. Intlekofer, A. M. *et al.* Effector and memory CD8+ T cell fate coupled by T-bet and eomesodermin. *Nat. Immunol.* **6**, 1236–44 (2005).

37. Townsend, M. J. *et al.* T-bet regulates the terminal maturation and homeostasis of NK and Vα14i NKT cells. *Immunity* **20**, 477–94 (2004).

38. Beyer, T. *et al.* Integrating signals from the T-cell receptor and the interleukin-2 receptor. *PLoS Comput. Biol.* **7**, e1002121 (2011).

39. Jones, N. *et al.* Akt and STAT5 mediate naïve human CD4+ T-cell early metabolic response to TCR stimulation. *Nat. Commun.* **10**, 2042 (2019).

40. Ranganath, S. & Murphy, K. M. Structure and Specificity of GATA Proteins in Th2 Development. *Mol. Cell. Biol.* **21**, 2716–25 (2002).

41. Kang, C. *et al.* The DNA damage response induces inflammation and senescence by inhibiting autophagy of GATA4. *Science.* **349**, aaa5612 (2015).

42. Schmid, M., Durussel, T. & Laemmli, U. K. ChIC and ChEC: Genomic mapping of chromatin proteins. *Mol. Cell* **16**, 147–57 (2004).

43. Skene, P. J. & Henikoff, S. A simple method for generating highresolution maps of genome-wide protein binding. *Elife* **4**, e09225 (2015).

44. Cousins, D. J., Lee, T. H. & Staynov, D. Z. Cytokine Coexpression During Human Th1/Th2

Cell Differentiation: Direct Evidence for Coordinated Expression of Th2 Cytokines. *J. Immunol.* **169**, 2498–2506 (2002).

45. Afgan, E. *et al.* The Galaxy platform for accessible, reproducible and collaborative biomedical analyses: 2016 update. *Nucleic Acids Res.* **46**, W537–W544 (2016).

Figure legends

Figure 1: Senescent CD4$^+$ EMRA T cells expressed high levels of GATA3 which correlates with increased mitochondrial mass.

(a) Representative flow cytometry histograms and cumulative graph of GATA3 staining in CD27/CD45RA defined CD4$^+$ T cell subsets (n=7). (b) Representative flow cytometry histograms and cumulative graph of Mitotraker Green staining in CD27/CD45RA defined CD4$^+$ T cell subsets (n=14). (c) Electron microscope images of CD27/CD45RA defined CD4$^+$ T cell subsets imaged directly *ex vivo*. Scale bars 1 µM. (d) Graph shows the percentage by cell volume of mitochondria in CD27/CD45RA defined CD4$^+$ T cell subsets determined by a point counting grid method from 20 different electron microscope images. (e) PGC1α staining in CD45RA/CD27 defined CD4$^+$ T cell subsets (n=8).

Figure 2: CD4$^+$ EMRA T cells have hyperpolarised mitochondria but maintain normal T cell metabolism.

(a) Mitochondrial membrane potential (MMP) was determined in CD27/CD45RA defined CD4+ T cell subsets using TMRE (n=10). Low MMP = red, intermediate MMP = blue, high MMP = green. (b) ROS production was obtained using DHE in the CD27/CD45RA defined CD4$^+$ T cell subsets (n=7). (c) OCR of the CD4$^+$ T cell subsets was measured after 15 minute stimulation with 0.5 µg/ml anti-CD3 and 5 ng/ml IL-2, cells were subjected to a mitochondrial stress test using indicated mitochondrial inhibitors. Data are representative of 4 independent experiments. (d) Basal OCR, (e) Basal ECAR and (f) the SRC of the CD4$^+$ T cell subsets after 15 minute stimulation with 0.5 µg/ml anti-CD3 and 5 ng/ml IL-2 (n=4).

Figure 3: DNA damage recruits a GATA-3-PGC1α complex to induce mitochondria biogenesis in CD4$^+$ EMRA T cells.

(a) DNA damage in the CD27/CD45RA defined CD4$^+$ T cell subsets was determined by assessing the

percentage of γH2AX positive cells and the p53:p-p53 ratio (n=6). (b) DNA damage in $CD4^+$ T cell subsets following the induction of oxidative stress using H_2O_2 (n=4). (c) Western blot showing Chk1 immunoprecipitation in the CD27/CD45RA defined $CD4^+$ T cell subsets quantifying the presence of GATA3 and PGC1α bound to the Chk1 antibody (n=3). (d) Chromatin immunocleavage showing GATA3 binding to the promoter regions of NRF1, NRF2, SOD3, and PGC1α in naïve $CD4^+$ T cells. (e) Tom20 and GATA3 staining in $CD4^+$ T cells following treatment with hydroxyurea (n=3). (f) Western blot showing GATA3 immunoprecipitation in $CD4^+$ T cells following hydroxyurea treatment quantifying the presence of PGC1α, NRF2 and SOD3 (n=3). (g) Representative flow cytometry histograms and graph of mitochondrial mass measured using mitotracker green following treatment of $CD4^+$ T cells with and without hydroxyurea and AZD6738 (n=4).

Figure 4: GATA3 and AMPK regulate $CD4^+$ T cell metabolism and mitochondrial biogenesis.

Graphs showing (a) PGC1α and (b) Mitotracker Green staining in whole $CD4^+$ T cells transfected with either control or GATA3 siRNA (n=5 and 6 respectively). (c) Tom20 confocal staining in Jurkat T cells transfected with either control or GATA3 siRNA (n=3). (d) MMP was determined in whole $CD4^+$ T cells transfected with either control or GATA3 siRNA using TMRE (*n* = 6). Low MMP = red, intermediate MMP = blue, high MMP = green. (e) OCR of whole CD4+ T cells transfected with either control or GATA3 siRNA was measured after 15 minute stimulation with 0.5 µg/ml anti-CD3 and 5 ng/ml IL-2, cells were subjected to a mitochondrial stress test using indicated mitochondrial inhibitors. Data are representative of 3 independent experiments. (f) Basal OCR and the SRC, together with ECAR following treatment with oligomycin (g) of the $CD4^+$ siRNA transfected cells stimulated as described above (n=3). (h) ex-vivo staining of pAMPK (Thr172) in CD27/CD45RA defined CD4+ T cell subsets (n=5). (i) Chromatin immunocleavage showing GATA3 binding to the promoter regions of PRKAA1, PRKAA2 in naïve $CD4^+$ T cells. (j) Potential mechanism of GATA3 and AMPK leading to mitochondrial biogenesis during DNA damage. (k) Quantification of mitochondrial

mass measured using mitotracker green, and assessment of ROS production using mitoSOX. Together with apoptosis measured by annexin V staining (l) following treatment of $CD4^+$ T cells with and without hydroxyurea and doxycycline (n=4).

Figure 1.

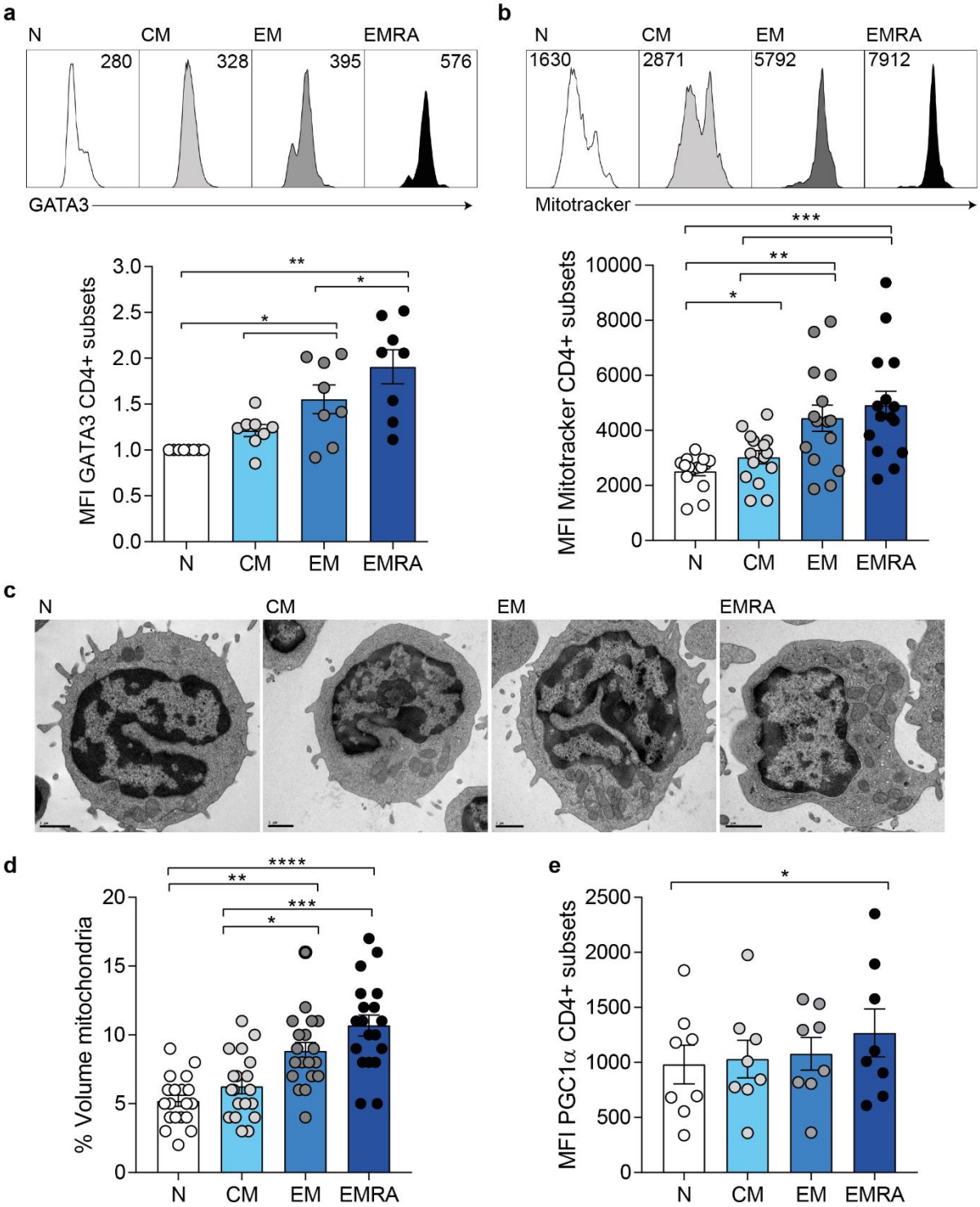
a
N
CM
EM
EMRA
280
328
395
576
GATA3
MFI GATA3 CD4+ subsets
3.0
2.5
2.0
1.5
1.0
0.5
0.0
**
*
*
N
CM
EM
EMRA
b
N
CM
EM
EMRA
1630
2871
5792
7912
Mitotracker
MFI Mitotracker CD4+ subsets
10000
8000
6000
4000
2000
0
***
**
*
N
CM
EM
EMRA
c
N
CM
EM
EMRA
d
% Volume mitochondria
20
15
10
5
0
****
**
***
*
N
CM
EM
EMRA
e
MFI PGC1α CD4+ subsets
2500
2000
1500
1000
500
0
*
N
CM
EM
EMRA

Figure 2.

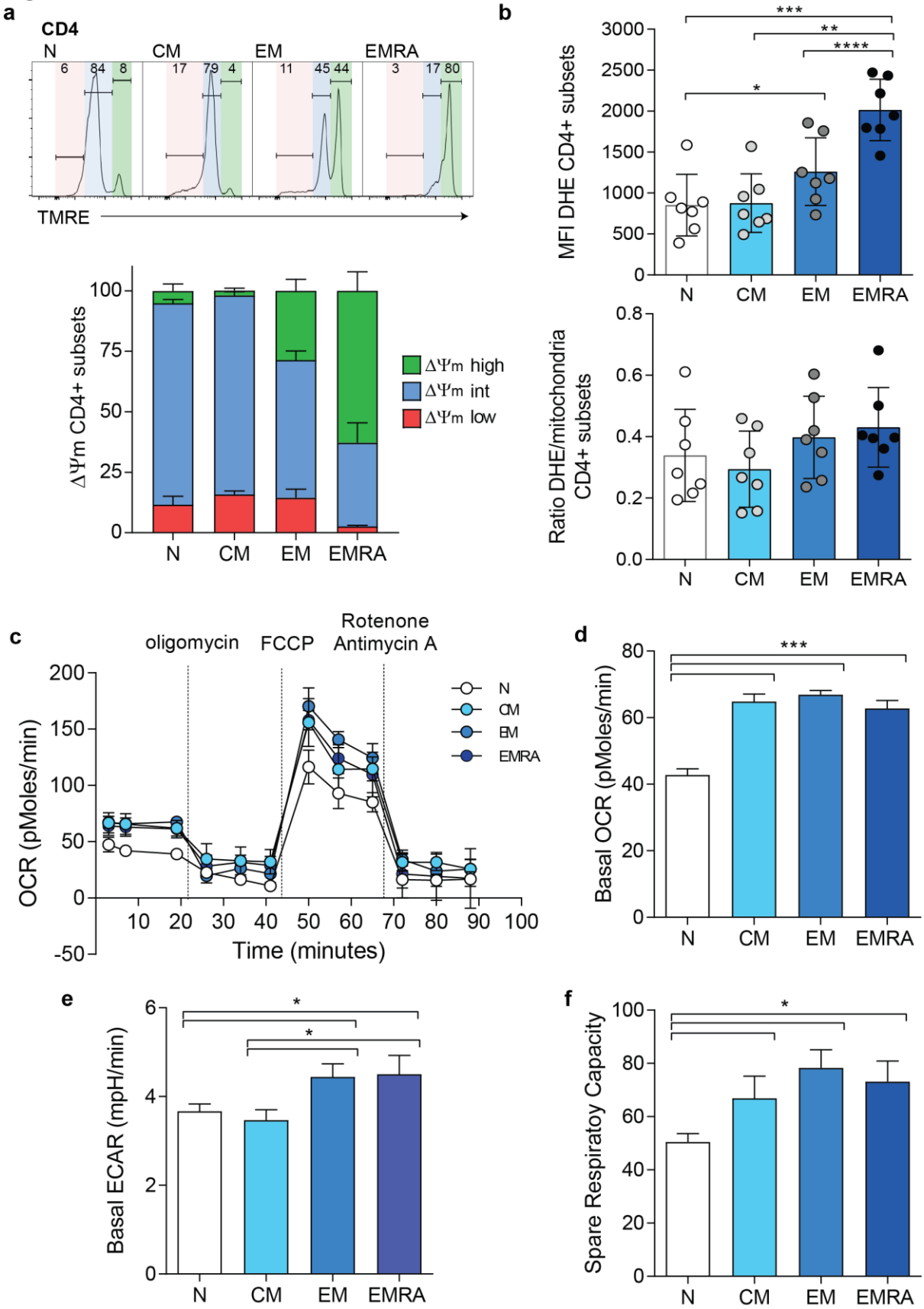
a
CD4
N
CM
EM
EMRA
6 84 8
17 79 4
11 45 44
3 17 80
TMRE
ΔΨm CD4+ subsets
ΔΨm high
ΔΨm int
ΔΨm low
b
MFI DHE CD4+ subsets
Ratio DHE/mitochondria CD4+ subsets
c
oligomycin
FCCP
Rotenone
Antimycin A
OCR (pMoles/min)
Time (minutes)
d
Basal OCR (pMoles/min)
e
Basal ECAR (mpH/min)
f
Spare Respiratoy Capacity

Figure 3.

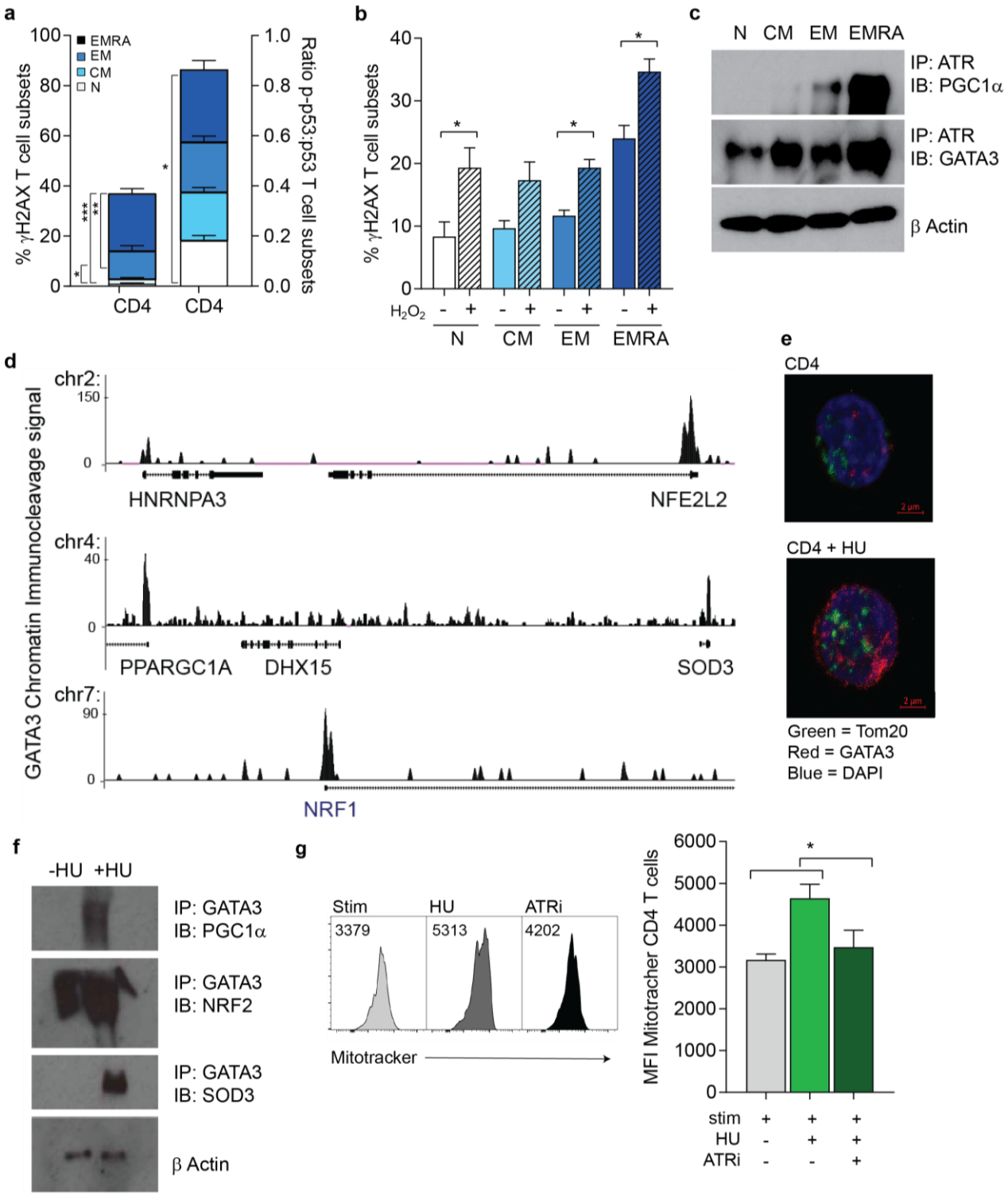
a
EMRA
EM
CM
N
% γH2AX T cell subsets
Ratio p-p53:p53 T cell subsets
CD4
CD4
b
% γH2AX T cell subsets
H2O2
N
CM
EM
EMRA
c
N CM EM EMRA
IP: ATR
IB: PGC1α
IP: ATR
IB: GATA3
β Actin
d
GATA3 Chromatin Immunocleavage signal
chr2:
HNRNPA3
NFE2L2
chr4:
PPARGC1A
DHX15
SOD3
chr7:
NRF1
e
CD4
CD4 + HU
Green = Tom20
Red = GATA3
Blue = DAPI
f
-HU +HU
IP: GATA3
IB: PGC1α
IP: GATA3
IB: NRF2
IP: GATA3
IB: SOD3
β Actin
g
Stim
HU
ATRi
3379
5313
4202
Mitotracker
MFI Mitotracher CD4 T cells
stim
HU
ATRi

Figure 4.

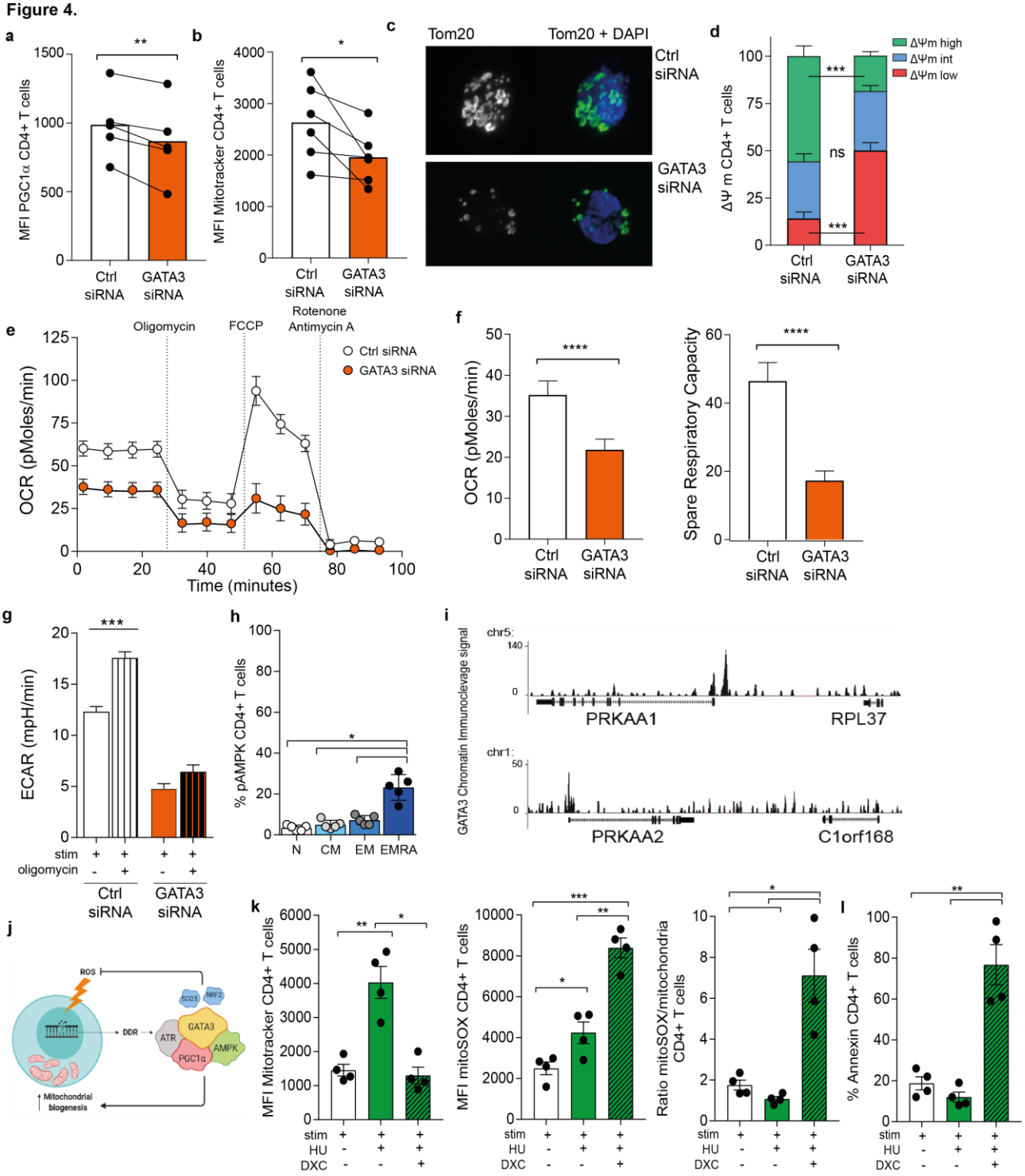
a
MFI PGC1α CD4+ T cells
Ctrl siRNA
GATA3 siRNA
b
MFI Mitotracker CD4+ T cells
c
Tom20
Tom20 + DAPI
Ctrl siRNA
GATA3 siRNA
d
ΔΨm high
ΔΨm int
ΔΨm low
ΔΨ m CD4+ T cells
ns
e
Oligomycin
FCCP
Rotenone
Antimycin A
Ctrl siRNA
GATA3 siRNA
OCR (pMoles/min)
Time (minutes)
f
OCR (pMoles/min)
Spare Respiratory Capacity
g
ECAR (mpH/min)
stim
oligomycin
h
% pAMPK CD4+ T cells
N
CM
EM
EMRA
i
GATA3 Chromatin Immunoclevage signal
chr5:
PRKAA1
RPL37
chr1:
PRKAA2
C1orf168
j
ROS
DDR
SOD3
NRF2
GATA3
ATR
AMPK
PGC1α
Mitochondrial biogenesis
k
MFI Mitotracker CD4+ T cells
MFI mitoSOX CD4+ T cells
Ratio mitoSOX/mitochondria CD4+ T cells
stim
HU
DXC
l
% Annexin CD4+ T cells

Extended data figure legends

Extended data figure 1: Expression of GATA3 in CD4$^+$ T cell subsets.

(a) Gating strategy for CD27/CD45RA defined CD4$^+$ T cell subsets. From left to right, lymphocytes, single cells, live cells, CD4$^+$ T cells and CD27/CD45RA subsets. (b) qPCR data showing the ΔCT relative expression of GATA3 in CD4$^+$ T cell subsets (n=3). (c) GATA3 staining in CD27/CD45RA defined CD4$^+$ T cell subsets with and without overnight stimulation with 0.5 µg/ml anti-CD3 (n=7) (d) GATA3 expression in unstimulated CD27/CD45RA defined CD8$^+$ T cell subsets (n=8). (e) Mitochondrial mass measured by mitotracker green staining in CD27/CD45RA defined CD4$^+$ T cell subsets with and without overnight stimulation as described above (n=8). (f) qPCR data showing the ΔCT relative expression of PGC1α in CD4$^+$ T cell subsets (n=3). (g) OCR of the CD4$^+$ T cells with and without 15 minute stimulation with 0.5 µg/ml anti-CD3 and 5 ng/ml IL-2, cells were subjected to a mitochondrial stress test using indicated mitochondrial inhibitors (n=3).

Extended data figure 2: Expression of GATA3 following hydroxyurea treatment

(a) Quantification of PGC1α and GATA3 following immunoprecipitation, shown as the ratio of PGC1α:βActin and GATA3:βActin (n=3). (b) Stain of p-p53 and the p53:p-p53 ratio following the induction of DNA damage by hydroxyurea in whole CD4$^+$ T cells. Mitotracker Green staining (c) and PGC1α (d) in CD4$^+$ T cells treated with and without hydroxyurea (n=5). (e) Quantification of GATA3 and mitochondrial mass by signal intensity from confocal data (n=3). (f) Quantification of PGC1α NRF1 and SOD3 following immunoprecipitation, shown as the ratio:βActin (n=3).

Extended data figure 3: siRNA knockdown of GATA3

(a) GATA3 siRNA transfection efficiency (n=6). (b) GATA3 staining following GATA3 siRNA transfection (n=3). (c) Percentage of live cells determined by Zombie NIR staining following GATA3 siRNA transfection (n=6). (d) Examples of PGC1α expression and mitochondrial mass following siRNA

transfection. (e) Mitochondrial mass and (f) mitochondrial volume analysis from confocal microscopy data (n=3). (g) OCR of whole $CD8^+$ T cells transfected with either control or GATA3 siRNA was measured after 15 minute stimulation with 0.5 µg/ml anti-CD3 and 5 ng/ml IL-2, cells were subjected to a mitochondrial stress test using indicated mitochondrial inhibitors (n=3).

Extended data figure 4. Chromatin immunocleavage and doxycycline treatment

(a) Chromatin immunocleavage showing GATA3 binding to the promoter regions of hexokinase 1/2 and SLC2A1 in naïve $CD4^+$ T cells. Representative examples of pAMPK staining ex-vivo (b) and after overnight stimulation (c) with 0.5 ug/ml aCD3. (d) Graph showing pAMPK expression in CD27/CD45RA defined stimulated $CD4^+$ T cell subsets (n=9). (e) Chromatin immunocleavage showing GATA3 binding to the promoter regions of c-myc. (f) Data showing c-myc expression in $CD4^+$ T cells following transfecting with either a control or GATA3 siRNA (n=4). (g) Representative examples of mitotracker and mitosox staining, together with annexin V staining (h) in $CD4^+$ T cells following incubation with hydroxyurea and doxycycline (n=4).

Extended data figure 1

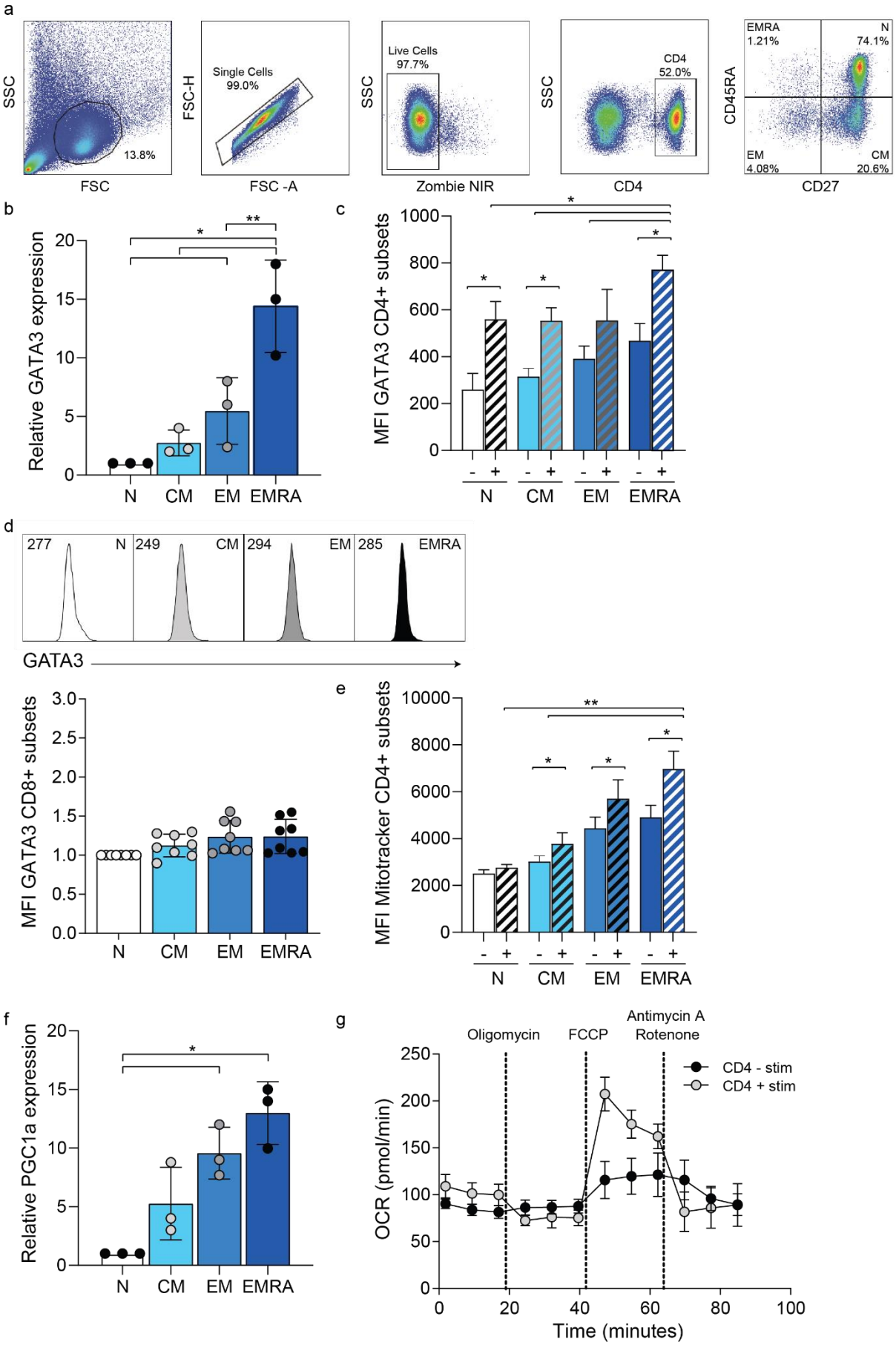

Extended data figure 2

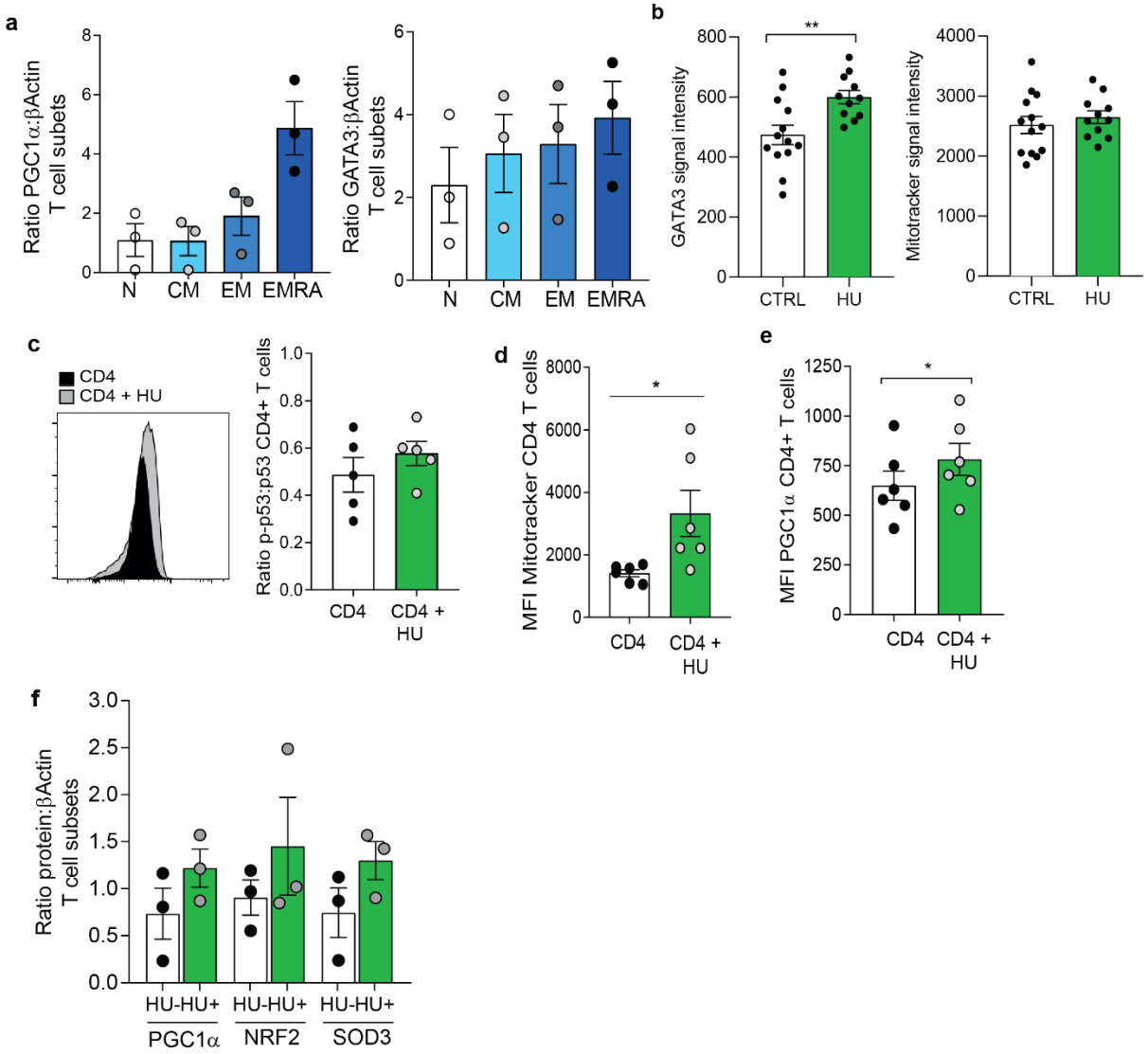

Extended data figure 3

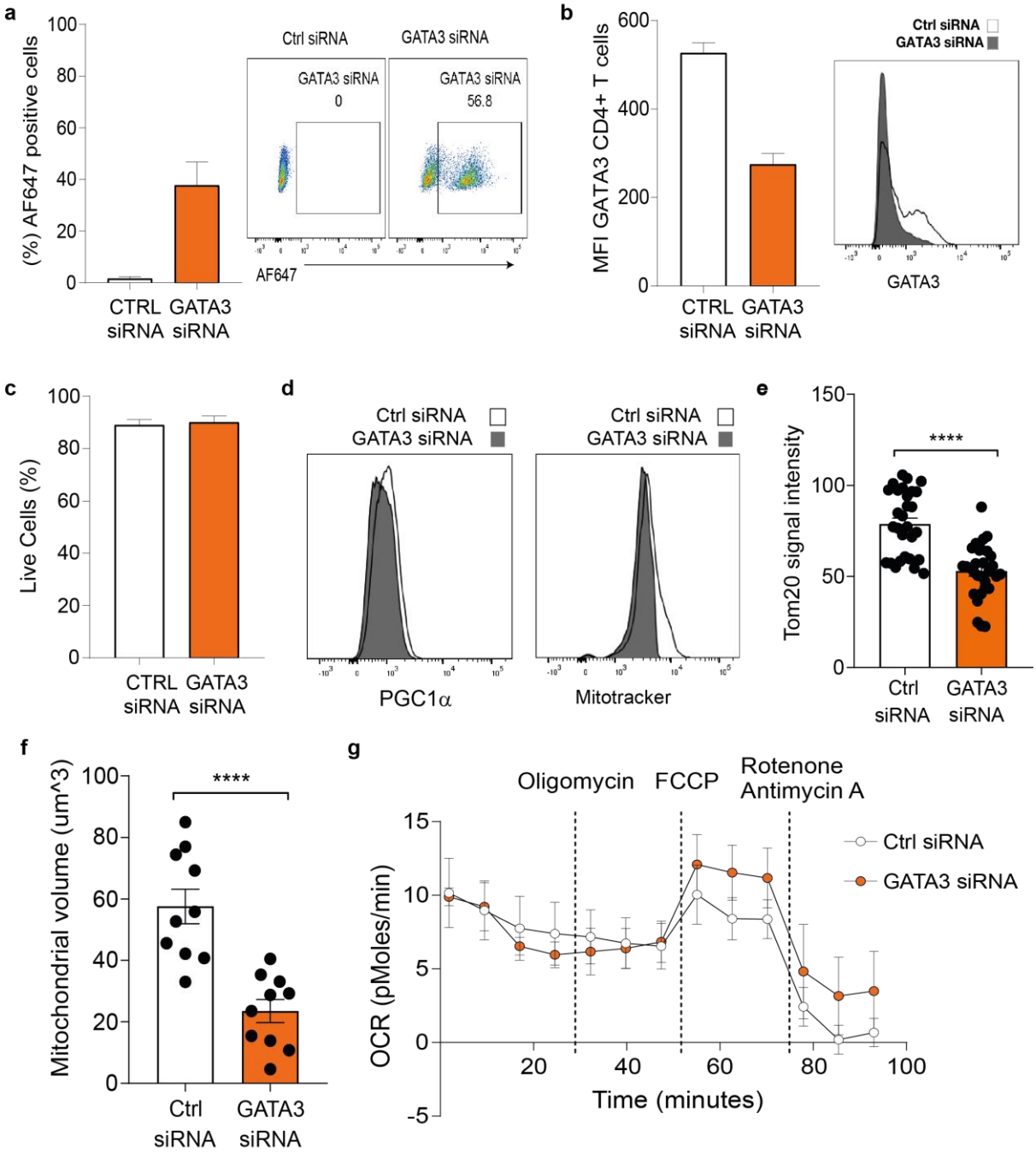
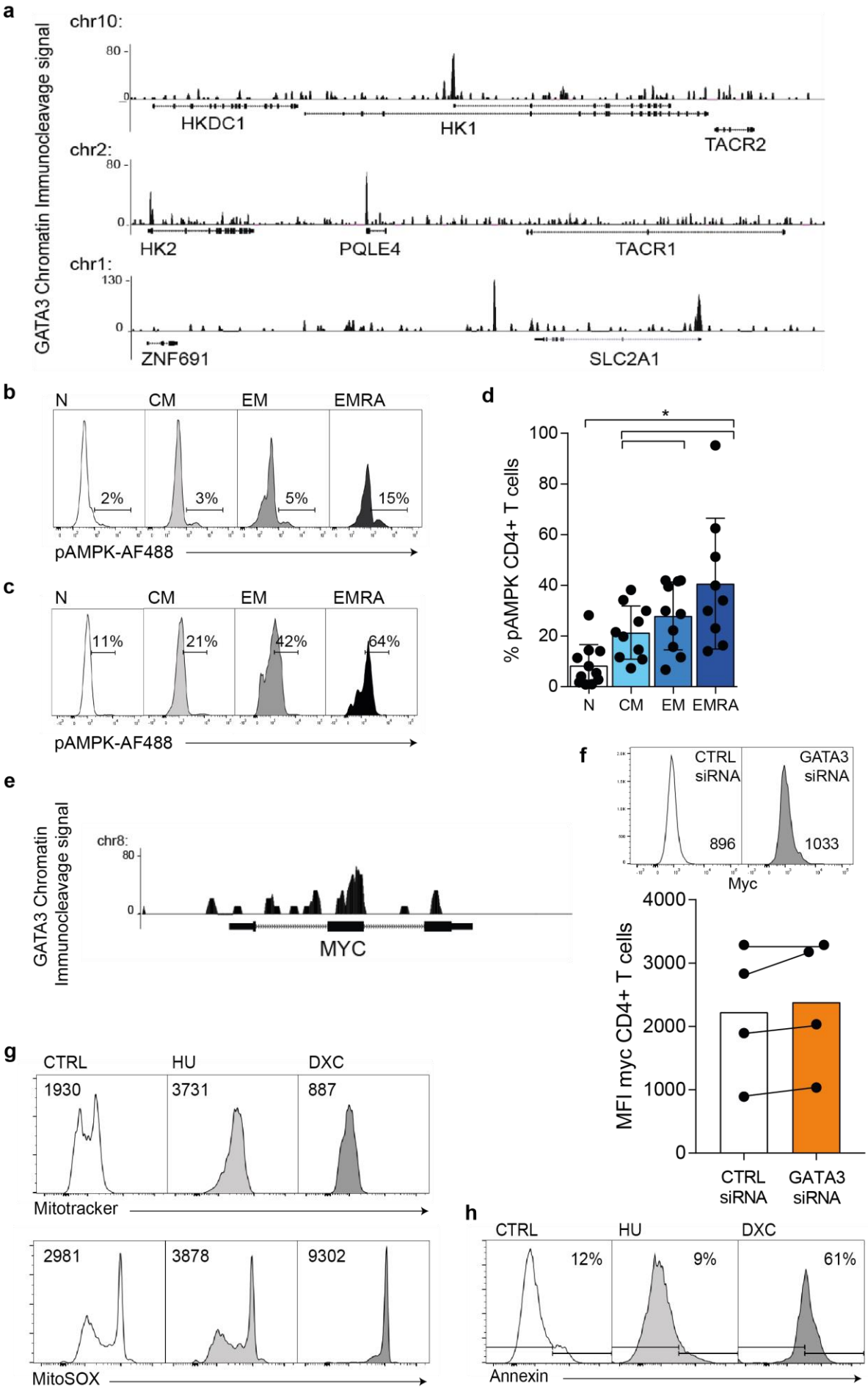
Extended data figure 4